Modeling vocal fold motion with a hydrodynamic semicontinuum model

M. Drew LaMar
Department of Mathematics, University of Texas at Austin, Austin, Texas 78712

Yingyong Qi
Qualcomm Inc., 5775 Morehouse Drive, San Diego, California 92121

Jack Xin[a)]
Department of Mathematics and TICAM, University of Texas at Austin, Austin, Texas 78712

Vocal fold (VF) motion is a fundamental process in voice production, and is also a challenging problem for numerical computation because the VF dynamics depend on nonlinear coupling of air flow with the response of elastic channels (VF), which undergo opening and closing, and induce internal flow separation. The traditional modeling approach makes use of quasisteady flow approximation or Bernoulli's law which ignores air compressibility, and is known to be invalid during VF opening. A hydrodynamic semicontinuum system for VF motion is presented. The airflow is modeled by a modified quasi-one-dimensional Euler system with coupling to VF velocity. The VF is modeled by a lumped two mass system with a built-in geometric condition on flow separation. The modified Euler system contains the Bernoulli's law as a special case, and is derivable from the two-dimensional compressible Navier–Stokes equations in the inviscid limit. The computational domain contains also solid walls next to VFs (flexible walls). It is shown numerically that several salient features of VFs are captured, especially transients such as the double peaks of the driving subglottal pressures at the opening and the closing stages of VF motion consistent with fully resolved two-dimensional direct simulations, and experimental data. The system is much simpler to compute than a VF model based on two-dimensional Navier–Stokes system. © *2003 Acoustical Society of America.* [DOI: 10.1121/1.1577547]

I. INTRODUCTION

Vocal folds (VF) are the source of the human voice, and their motion is a fundamental process in speech production. Since VF motion is mechanical and results from the interaction of airflow and elastic response of VF, partial differential equations (PDEs) can be written down from classical continuum mechanics based on our knowledge of VF structures and air flow characteristics. A model of VF motion is naturally made of a certain form of compressible Navier–Stokes equations coupled with an elastic system on VF deformation.

In the past decade, much progress has been made in modeling the elastic aspect of VF. There are by now a hierarchy of elastic models for VF, from the two mass model of Ishizaka and Flanagan,[1] Bogaert,[2] to 16 mass as well as the continuum model of Titze and co-workers.[3–7] However, the modeling of airflow or the fluid aspect of VF is less explored. There are broadly two types of approaches in treating the glottal flow. One is to combine the Bernoulli's law in the bulk of the flow (quasisteady flow approximation) with either a quasi-steady pressure recovery theory,[1] or an analytical approximation downstream of the flow separation point.[2,3,8] Bernoulli's law oversimplifies the flow in the sense that partial derivatives in time are ignored, however, they are not negligible for transient effects such as pressure peaks. For

example, it was realized[9] and concluded[10] that Bernoulli's law is not valid during one-fifth of the VF vibration cycle, especially at the VF opening and closure. The compressibility is ignored in the Bernoulli's law, especially in the subglottal region just before the VFs. The compressibility is essential for the pressure buildup to reopen the VFs.

The other approach is direct numerical simulation of channel flows and VF in the continuum. For example, Alipour *et al.*[6,7] simulated a two dimensional incompressible Navier–Stokes (NS) system and a finite element model of VF cover and body. Extensive computation and coding are expected to fully resolve the flows in the presence of moving boundaries, closures, and flow separation.

In this paper, we study an intermediate system consisting of a modified quasi-one-dimensional compressible Euler equations for the air flows and a recent version of the two mass model on VF.[2] The flow separation is accounted for using an empirical formula on the VF opening angle. The model is semicontinuum in that the flow variables are spatially continuous, while VFs are approximated by two masses (discrete). The modified quasi-one-dimensional Euler equations are extensions of those in the study of duct flows in aerodynamics,[11–14] with an additional coupling to the velocity of channel boundaries. This is the only viscous effect. It will be shown numerically that the modified Euler system is able to handle strong transient effects, such as rapid variation of subglottal pressures at VF opening and closing. Nu-

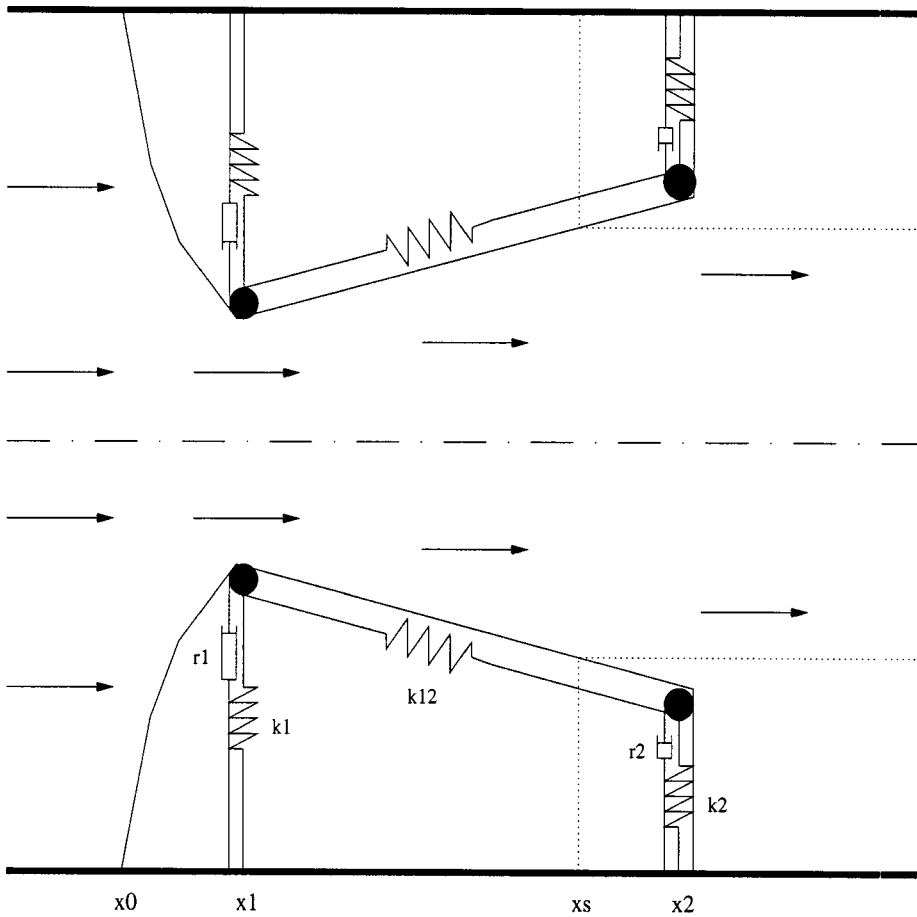[a)]Author to whom correspondence should be addressed; electronic mail: jxin@math.utexas.edu

FIG. 1. A sketch of the flow and the two mass model. The computational domain is $[x_0, x_2]$. The channel width is fixed at x_0, and smoothly interpolated to mass one over $[x_0, x_1]$; x_s is the separation point for diverging glottis.

merical simulation of the model is less technical and many salient features of VF dynamics[6,8,10,15–17] are captured.

The rest of the paper is organized as follows. In Sec. II, the model equations are introduced, and related modeling issues addressed. In Sec. III, numerical method, convergence, and simulation results are discussed. It is shown numerically that model solutions recover several known VF characteristics, for example, the double VF inlet pressure peaks at VF opening and closure. The model robustness is shown by varying subglottal input pressure and plotting how air volume velocity changes as a function of time. The conclusion is in Sec. IV, followed by the acknowledgments. Appendix A contains a derivation of the modified quasi-one-dimensional Euler equations. Appendix B shows a linear stability analysis on the existence of oscillation modes near flat fold, to demonstrate the role of the boundary velocity coupling term in the modified Euler equations.

II. THE SEMICONTINUUM MODEL

Suppose the larynx is a two-dimensional channel with a finite mass elastic wall of cross section width $A(x,t)$. The VF is lumped into a sum of two masses connected by a spring, and each mass is connected to the solid wall by a spring and a damper, the common scenario in the two mass model,[1,2] see Fig. 1. The air flows from $x=x_0$ to $x=x_2$, and is modeled by the modified quasi-one-dimensional Euler system.

Conservation of mass,

$$(A\rho)_t + (\rho u A)_x = 0, \tag{2.1}$$

ρ is the air density, u is the air velocity.

Reduced momentum equation,

$$(\rho u A)_t + (\rho u^2 A)_x = -(pA)_x + A_x p + \rho u A_t, \tag{2.2}$$

p is the air pressure.

Assuming that the temperature is maintained as constant, the airflow is isothermal,[18] and the equation of state is

$$p = a^2 \rho, \tag{2.3}$$

where a is the speed of sound. The cross section width A is a piecewise linear function in x determined by the displacements of the two masses (y_1, y_2), in the two-mass model system (Bogaert,[2] Ishizaka and Flanagan[1]):

$$m_1 y_1'' + r_1 y_1' + k_1(y_1 - y_{0,1}) + k_{12}(y_1 - y_2 + y_{0,12}) = F_1, \tag{2.4}$$

$$m_2 y_2'' + r_2 y_2' + k_2(y_2 - y_{0,2}) + k_{12}(y_2 - y_1 - y_{0,12}) = 0, \tag{2.5}$$

where $F_1 = L_g \int_{-L}^{x_s} p \, dx$, L_g the transverse (to the flow) dimension of VF, equal to 1 cm; y_i's are VF openings at locations x_i's, $i=1, 2$; $x_s = x_2$ if there is no flow separation, and $x_s =$ the location of flow separation if it occurs. The m_i, r_i, k_i, $i=1, 2$, are mass density, damping and elastic spring constants. Mass one (lower mass) is situated near the VF entrance, and mass two (upper mass) is located towards the exit of the glottal region. Following Bogaert,[2] x_s will be estimated by an empirical formula on the degree of diver-

gence of the VF. Our complete VF model is the coupled system (2.1)–(2.5).

The viscous effect in the flow produces the term $\rho u A_t$ from the no-slip boundary condition of the two-dimensional flows, see derivation in Appendix A. Without this term, the above system is quasi-one-dimensional Euler in gas dynamics.[11–14] The extra term introduces coupling to wall velocity, and is critical in transferring energy from airflow into the VF, as the Titze theory[19] predicted. Appendix B shows that with this term, there exist oscillation modes near flat fold under a threshold condition similar to the one in Titze.[19] For simplicity, we ignored other viscous effects.

The two-mass model (2.4)–(2.5) is a recent improvement[2] of the original IF72[1] in that the flow separation point is not always at the VF exit, instead it depends on the glottal geometry. Flow separation basically refers to a change of flow behavior from being attached to the VF cover via a viscous boundary layer to a developed free jet with vortical structures and turbulent wake. Because of the vortical buildup, pressure near the wall is typically low, and can be approximated by setting it to zero (or ambient pressure) as done on mass two in (2.5). In converging glottis, there is no flow separation, however in diverging glottis, it occurs if the diverging angle is large enough. It is expedient for our modeling purpose to adopt a working hypothesis supported by experiments[2,8]

$$y_2/y_1 < 1.1 \Rightarrow x_s = x_2, \tag{2.6}$$

$$y_2/y_1 > 1.1 \Rightarrow x_s = x_1 + \frac{(x_2-x_1)y_1}{10(y_2-y_1)}, \quad y_s = 1.1y_1. \tag{2.7}$$

Notice that the location of the flow separation is a variable depending on the diverging angle. It is worth pointing out that the assumptions made for deriving the reduced flow model are more accurate prior to the separation point. After the flow separation point, the reduced flow model needs to be properly corrected. For example, contribution of the viscous boundary layers can be introduced in the model to calculate the separation point more accurately than formula (2.6)–(2.7), and take into account the energy losses downstream of the separation point. A formulation of such a treatment with von Karman equations is given by Pelorson *et al.*[8] For simplicity of the model, we shall not pursue this task here, instead we rely on (2.6)–(2.7) as a simple way to incorporate separation effects. As the pressure after separation point is not contributing a force to the upper mass in (2.5), modeling error of ignoring viscous losses in the boundary layers is minimized within our model system. Viscous effects can be neglected upstream of the separation point for vocal flows.[8]

We also adopt the elastic collision (stopping) criterion[1,2] when the two sides of VF approach each other and close. When y_i's are smaller than a critical level y_c, then VF is considered closed, and (m_i, r_i, k_i) $(i=1,2)$ are adjusted to closure values.[1,2] In this case, the flow equations are solved only over $x \in [x_0, x_1]$, and in (2.4)–(2.5) the pressure force is adjusted to $F_1 = L_g \int_{x_0}^{x_1} p\, dx$. Due to constant input pressure p_0 at x_0, pressure at x_1 builds up. The two mass ODE's

(ordinary differential equations) are still running even during VF closure, and in due time the increased pressure reopens VF.

The two-mass model by Bogaert[2] consists of (2.4)–(2.7) along with the above elastic collision criterion. In Bogaert,[2] the forcing term on mass one F_1 is calculated with the Bernoulli's law in the open glottis case. In the closed glottis case, air pressure is equal to the ambient pressure over $[x_0, x_s]$. The two mass parameters are as listed in the table.

Our VF model system is solved as an initial boundary value problem on $x \in [x_0, x_2]$. The initial conditions are $p(x,0) = 0.14$ Pa, the ambient air pressure; $u(x,0) = 0$; $(y_1, y_2)(0) = (y_{0,1}, y_{0,2})$, the equilibrium two-mass position. The inlet boundary conditions are $(p,u)(x_0,t) = (p_0(t), u_0(t))$, where $p_0(t)$ is a smooth increasing function such that $p_0(0) = 0.14$ Pa, $p_0(0.1) = 700$ Pa; $u_0(t)$ is a smooth increasing function such that $u_0(0) = 0$, $u_0(0.1) = 0.114\,285a$, a is the speed of sound. The outlet boundary condition is $(p_x, u_x)(x_2, t) = 0$. The advantage of such Neumann-type boundary conditions is to help the flow to go out of the computational domain, and minimize numerical boundary artifacts.

The major difference between our model and that of Bogaert[2] is that we do not make quasisteady approximation on the flow variables, instead we integrate the time-dependent system (2.1)–(2.2). This turns out to be particularly important for capturing transients near closure and reopening stages of VF motion. It is helpful to put the system (2.1)–(2.2) into a rescaled form. Let $v = u/a$, a is the speed of sound. Then,

$$\frac{1}{a}(Ap)_t + (pvA)_x = 0,$$

$$\frac{1}{a}(pvA)_t + (pv^2A)_x = -(pA)_x + A_xp + pvA_t/a, \tag{2.8}$$

where typically $v = u/a \approx 0.1$, the Mach number. If we use the convenient cm g ms unit, $a = 35$ cm/ms, $1/a$ is a small parameter. If we ignore the terms with a, we have exactly Bernoulli's law for quasisteady flows. These seemingly small terms are essential especially during opening stage of VF, and should be kept for an accurate time-dependent solution.

III. NUMERICAL METHOD AND SIMULATION RESULTS

For given VF shape, $A(x,t)$, the flow system (2.1)–(2.2) is of the form

$$U_t + (F(U))_x = G(U), \tag{3.1}$$

the so-called conservation law (see Ref. 18 and references therein) with lower order source term G. The function F is the flux function. We implemented a first-order finite difference method, where time marching is split into two steps. In the first step $(t = nk \rightarrow (n+\frac{1}{2})k)$, we solve the conservation law $U_t + (F(U))_x = 0$ with explicit Lax–Friedrichs method,[18]

$$U_j^{n+1/2} = \frac{1}{2}(U_{j-1}^n + U_{j+1}^n) - \frac{k}{2h}(F(U_{j+1}^n) - F(U_{j-1}^n)), \tag{3.2}$$

TABLE I. Two mass model parameters in cgs unit.

m_1	0.17 g
m_2	0.03 g
$x_2 - x_1$	0.2 cm
$x_1 - x_0$	0.05 cm
$k_{1,open}$	45 kdynes
$k_{1,closed}$	180 kdynes
$y_{0,1}$	0 cm
$k_{2,open}$	8 kdynes
$k_{2,closed}$	32 kdynes
$y_{0,2}$	0.0 cm
k_{12}	25 kdynes
$y_{0,12}$	0 cm
y_c	0.001 cm
$A(x_0, t)$	2 cm
$r_{1,open}$	17.5 dynes/(cm s)
$r_{1,closed}$	192.4 dynes/(cm s)
$r_{2,open}$	18.6 dynes/(cm s)
$r_{2,closed}$	49.6 dynes/(cm s)

FIG. 3. A simulated VF vibration cycle, similar to the figure on p. 113 of Sataloff (Ref. 21).

where k and h are time step and spatial grid size. Here k must be small enough to ensure stability of the difference scheme and to keep the computed flow velocity positive (no back flow is allowed). In step two $((n + \frac{1}{2})k \rightarrow (n+1)k)$, we update the solution from $U^{n+\frac{1}{2}}$ to U^{n+1} by implicitly integrating ODEs: $U_t = G(U)$ in the flow equations, and the two-mass equations (2.4)–(2.5); where we apply central differencing in space and backward differencing in time. In the first step, U is updated using VF shape A at time $t = nk$; in the second step, the ODEs of the two-mass system and source terms are solved to update solutions to $(n +1)k$. We point out that when VF approach closure, the ODE's in step two become rather stiff, and this is the main reason to use implicit backward differencing in time.[20]
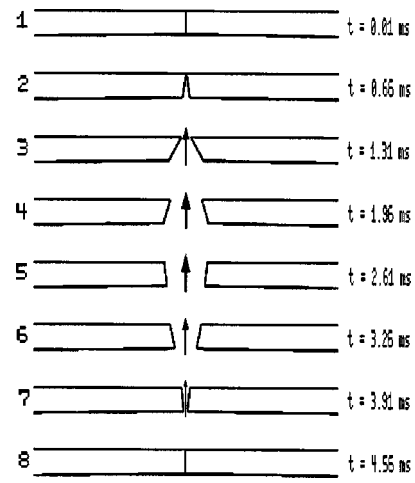
The numerical parameters used in our computation are

space grid size $h = 0.25/(nx - 1)$, where the computational domain is $x_2 - x_0 = 0.25$ cm, nx the total number of spatial grid points, $nx \geq 80 \, (h \leq 0.003 \, 165)$; time step $k \leq 10^{-7}$. The time unit is ms, length unit cm, speed of sound $a = 35$ cm/ms. The two mass model parameters are listed in Table I. A convergence test of numerics is shown in the plot of the air volume velocity passing through the glottis as a function of time in Fig. 2. The numerical grids $h = 0.001 \, 572 \, 3 \, (nx = 160)$, $k = dt = 2.5 \times 10^{-8}$ are used for the rest of the runs.

Now we describe our numerical results, and compare with figures in the literature either from experimental measurements or model calculations. In Fig. 3, we show a cycle of VF vibration, which resembles well the figure on p. 113 of Sataloff's *Scientific American* article.[21]
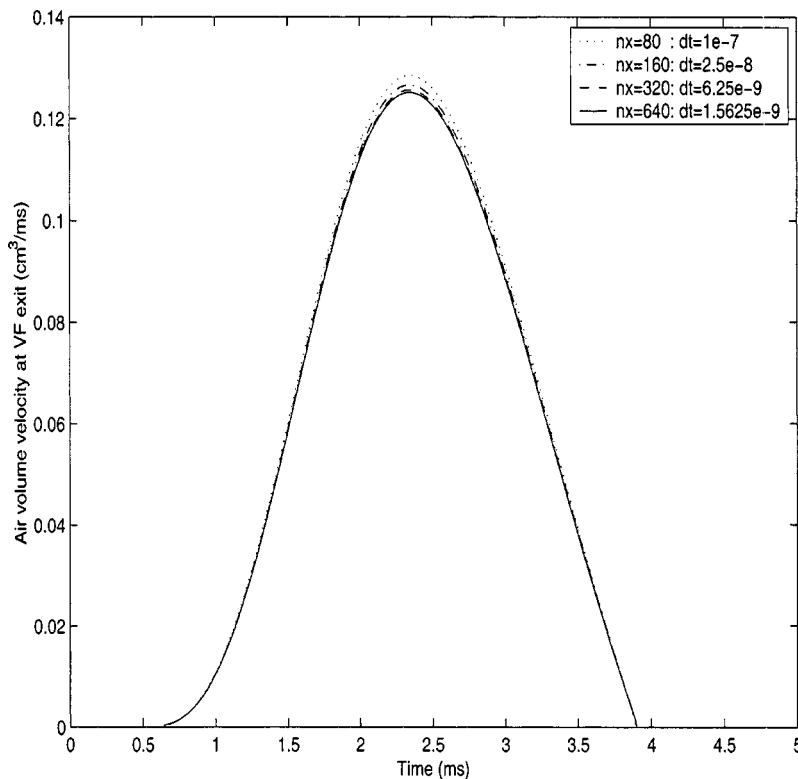

FIG. 2. The air volume velocity at VF exit x_2 to show convergence of numerical solutions under grid refinement.
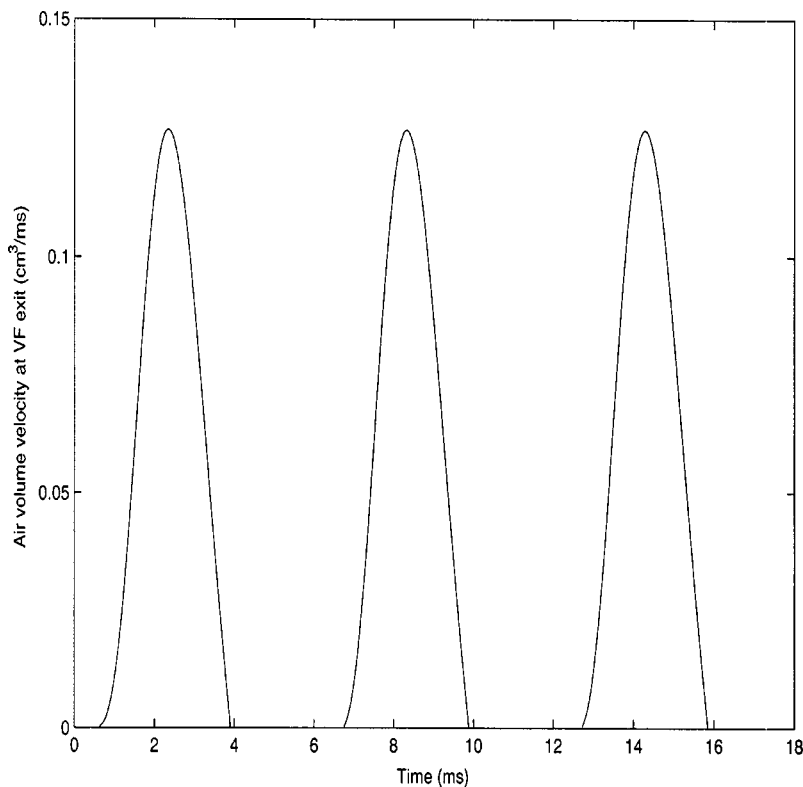
FIG. 4. Simulated VF air volume velocity (cm^3/ms) vs time at exit of VF from model (2.1)–(2.5).

In Fig. 4, we show the computed air volume velocity at the exit of VF, similar to Fig. 6, Fig. 7, Fig. 8 of Story and Titze,[3] and Fig. 6 of Alipour and Scherer.[6] Note that the pressure recovery downstream of the separation point is considered in the former,[3] and that a 2D incompressible NS calculation is used on a numerical domain covering a considerable wake flow region beyond x_2 in the latter[6] (see Fig. 4, p. 474). This comparison lends indirect support to the efficiency of our model treatment of VF flows.

Figure 5 is the experimentally measured intraglottal pressure on an excised canine larynx from Titze[15] (see also Jiang and Titze[16]), which showed the double peak (intraglottal) pressure structure, respectively, at VF opening and closing. Figure 6 is our computed subglottal pressure before mass one. The double peaks are present and resemble those

in Fig. 5, except that our second peak has a similar width as the first peak. Two main factors contribute to the difference. One is that the experiments have measured contact pressure when VFs are closed, and air pressure when VFs are open. Their intraglottal pressure has both components, while our computed subglottal pressure is only air pressure. As a result, the second peak in experiments due to air-pressure's gradual change is wider than the first which is mainly contact pressure. The other is that the closure treatment of two mass model differs from the actual VF closure. Our subglottal pressure is also in qualitative agreement with the computed subglottal air pressure in Fig. 5 (bottom frame),[6] which showed two peaks of nearly equal widths as well. Double peaks of intraglottal pressures have been computed[3] with a three-mass body-cover model and considerations of experimental conditions.

We also tested our model robustness under input pressure variation. In Fig. 7, we show a plot of air volume velocity vs time at VF exit for three subglottal pressures at x_0: 700 Pa, 1400 Pa, 2100 Pa with other parameters the same. We see that as subglottal pressures increase with other parameters fixed, air volume velocity curves get higher (at the peaks) and steeper (at the two sides). This agrees very well with Fig. 2.14(a), p. 78, of Stevens,[17] and is another support for our model.

We extend the flow domain to 0.5 cm downstream of x_2 (Fig. 1). Figure 8 shows the transglottal pressure as a function of time, calculated as the absolute difference between the instantaneous subglottal and supraglottal pressure values. The first and second peaks correspond to the opening of the glottis at mass 1 and 2, respectively, while the third peak corresponds to the closing of the glottis. The figure is similar to Fig. 5 in Alipour and Scherer,[6] as well as Fig. 9 of Austin
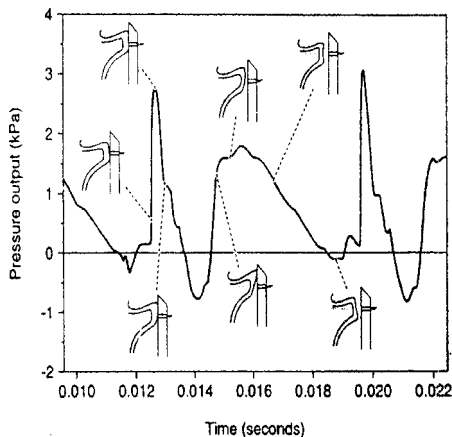

FIG. 5. Experimentally measured intraglottal pressure on excised canine larynx, reproduced Fig. 8 on p. 426 of Titze (Ref. 11) (with permission of the author and the publisher).
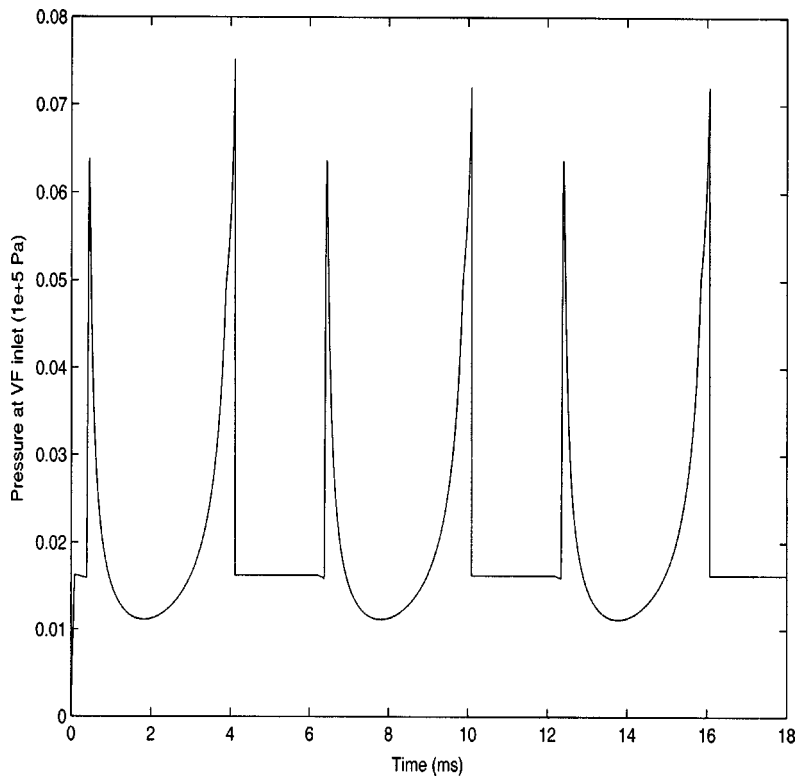
FIG. 6. The air pressure at VF inlet (before lower mass) versus time.

and Titze,[22] which displays experimental data collected from human subjects.

IV. CONCLUDING REMARKS

In this paper, we introduced and computed a semicontinuum VF model consisting of a modified quasi-one-dimensional Euler system and a recent two-mass model.[2] The flow part of the model is more accurate than a traditional treatment with Bernoulli's law, and also much simpler than a full two-dimensional Navier–Stokes system. We demonstrated numerical convergence and that the model solutions are in qualitative agreement with known VF characteristics.
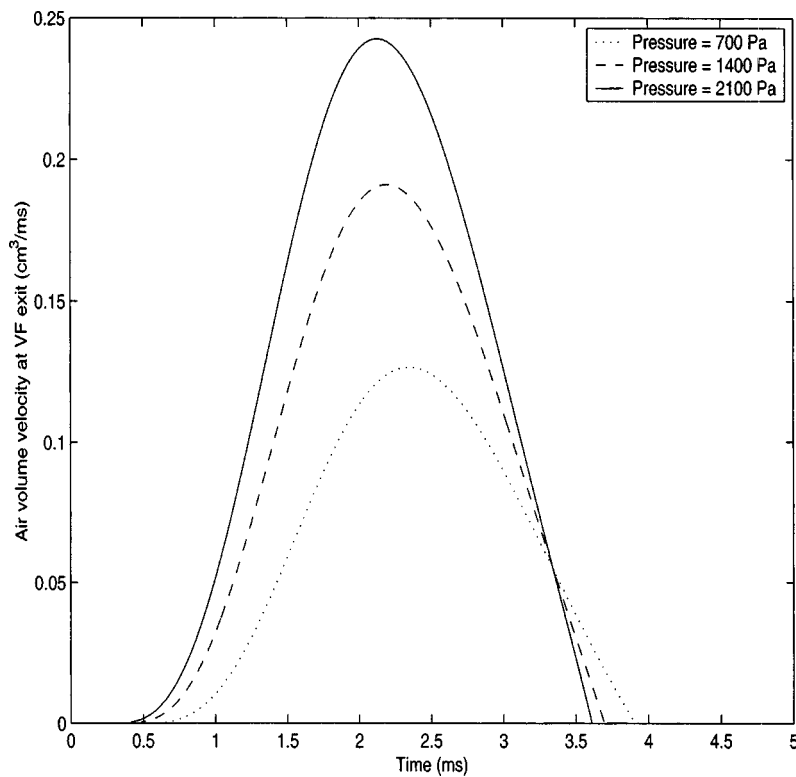

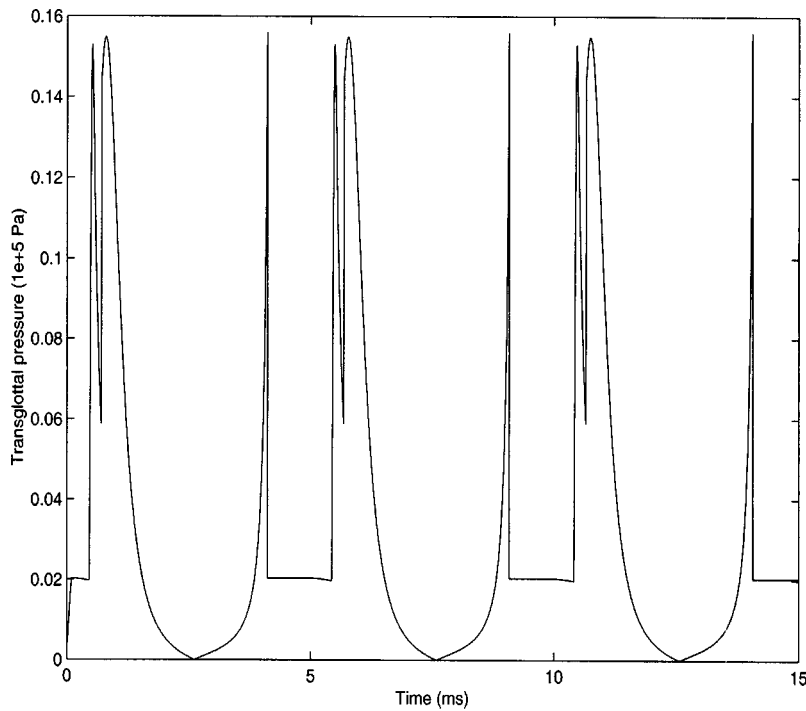FIG. 7. The air volume velocity at x_2 for three values of the input subglottal pressures at x_0.

LaMar *et al.*: Modeling vocal fold motion

FIG. 8. Transglottal pressure through an extended domain, 0.5 cm past x_2 in Fig. 1.

ACKNOWLEDGMENTS

APPENDIX A: DERIVATION OF MODIFIED EULER SYSTEM

We derive the fluid part of the model system assuming that the fold varies in space and time as $A = A(x,t)$. Consider a two-dimensional slightly viscous subsonic air flow in a channel with spatially temporally varying cross section in two space dimensions, $\Omega_0 = \Omega_0(t) = \{(x,y):x \in [-L,L], y \in [-A(x,t)/2, A(x,t)/2]\}$, where $A(x,t)$ denotes the channel width, or cross sectional area as the third dimension is uniform. The two-dimensional Navier–Stokes equations in differential form are (Batchelor,[23] p. 147) as follows.

Conservation of mass,

$$\rho_t + \nabla \cdot (\rho \vec{u}) = 0. \tag{A1}$$

Conservation of momentum,

$$(\rho \vec{u})_t = -\nabla \cdot (\rho(\vec{u} \otimes \vec{u})) + \text{div}(\sigma \cdot \vec{n}), \tag{A2}$$

where σ is the stress tensor, $\sigma = (\sigma_{ij}) = -p\delta_{ij} + d_{ij}$, and

$$d_{ij} = 2\mu \left(e_{ij} - \frac{\text{div} \vec{u}}{3} \delta_{ij} \right),$$

$$e_{ij} = \tfrac{1}{2}(u_{i,x_j} + u_{j,x_i}),$$

$$(x_1, x_2) \equiv (x,y),$$

μ is the fluid viscosity, $\Omega(t)$ is any volume element of the form $[\vec{u} = (u_1, u_2)]$

$$\Omega(t) = \{(x,y): x \in [a,b] \subset [-L,L],$$
$$y \in [-A(x,t)/2, A(x,t)/2]\}. \tag{A3}$$

The equation of state is either polytropic or isothermal.
The boundary conditions on $(\rho, \vec{u})$ are as follows:

(1) on the upper and lower boundaries $y = \pm A(x,t)/2$, $\rho_y = 0$, and $\vec{u} = (0, \pm A_t/2)$, the velocity no slip boundary condition;
(2) at the inlet, $x = -L$, $p = p_0$, given subglottal pressure $(u_1, u_2) = (u_{1,0}, u_{2,0})$, given input flow velocity. At the exit $(p, u_1, u_2)_x = 0$, to help the waves go out of the domain freely.

We are only concerned with flows that are symmetric in the vertical. For positive but small viscosity, the flows are laminar in the interior of Ω_0 and form viscous boundary layers near the upper and lower edges. The vertically averaged flow quantities are expected to be much less influenced by the boundary layer behavior as long as $A(x,t)$ is much larger than $O(\mu^{1/2})$.

Let us assume that the flow variables obey

$$|u_{1,y}| \ll |u_{1,x}|,$$

$$|u_{2,y}| \ll |u_{1,x}|, \quad \text{away from boundaries of } \Omega_0,$$

$$|\vec{u}_y| \gg |\vec{u}_x|, \quad \text{near the boundaries of } \Omega_0, \tag{A4}$$

$$|\rho_y| \ll |\rho_x|, \quad \text{throughout } \Omega_0.$$

These are consistent with physical observations in the viscous boundary layers (Batchelor,[23] p. 302), namely, there are large vertical velocity gradients, yet small pressure or density gradients in the boundary layers. The boundary layers are of width $O(\mu^{1/2})$. Denote by $\bar{\rho}$, $\bar{u}_1$, the vertical averages of ρ and u_1. Note that the exterior normal $\vec{n}=(-A_x/2,1)/(1+A_x^2/4)^{1/2}$ if $y=A/2$, $\vec{n}=(-A_x/2,-1)/(1+A_x^2/4)^{1/2}$ if $y=-A/2$.

Let $a=x$, $b=x+\delta x$, $\delta x \ll 1$, t slightly larger than t_0. We have

$$\frac{d}{dt}\int_{\Omega(t)}\rho\,dV=\frac{d}{dt}\int_{\Omega(t_0)}\rho J(t)dV$$

$$=\int_{\Omega(t_0)}\rho_t J(t)dV+\int_{\Omega(t_0)}\rho J_t\,dV,\qquad(A5)$$

where $J(t)$ is the Jacobian of volume change from a reference time t_0 to t. Since $\Omega(t)$ is now a thin slice, $J(t)=A(t)/A(t_0)$ for small δx, and $J_t=A_t(t)/A(t_0)$. The second integral in (A5) is

$$\int_{\Omega(t_0)}\rho J_t\,dV=\bar{\rho}\frac{A_t(t)}{A(t_0)}A(t_0)\delta x=\bar{\rho}A_t(t)\delta x.\qquad(A6)$$

The first integral is simplified using (A1) as

$$\int_{\Omega(t_0)}\rho_t J(t)dV=\int_{\Omega(t)}\rho_t\,dV=-\int_{\partial\Omega(t)}\rho\vec{u}\cdot\vec{n}\,dS.\qquad(A7)$$

We calculate the last integral of (A7) further as follows:

$$\int_{\partial\Omega}\rho\vec{u}\cdot\vec{n}\,ds=\int_{-A/2}^{A/2}(-\rho u_1)(x,y,t)dy+\int_{-A/2}^{A/2}(\rho u_1)$$

$$\times(x+\delta x,y,t)dy+\int_x^{x+\delta x}\rho\cdot(0,A_t/2)$$

$$\cdot(-A_x/2,1)dx+\int_x^{x+\delta x}\rho$$

$$\cdot(0,-A_t/2)\cdot(-A_x/2,-1)dx$$

$$=\overline{\rho u_1}A|_x^{x+\delta x}+\frac{\delta x}{2}(\rho A_t)|_{y=A/2}$$

$$+\frac{\delta x}{2}(\rho A_t)|_{y=-A/2}+O((\delta x)^2)$$

$$\approx(\bar{\rho}\cdot\bar{u}_1A)|_x^{x+\delta x}+\bar{\rho}A_t\delta x+O((\delta x)^2),\qquad(A8)$$

where we have used the smallness of ρ_y to approximate $\rho|_{y=\pm A/2}$ by $\bar{\rho}$ and $\overline{\rho u_1}$ by $\bar{\rho}\cdot\bar{u}_1$. Combining (A5)–(A7), (A8) with

$$\frac{d}{dt}\int_{\Omega}\rho\,dV=(\bar{\rho}A\,\delta x)_t+O((\delta x)^2),\qquad(A9)$$

dividing by δx and sending it to zero, we have

$$(\bar{\rho}A)_t+(\bar{\rho}\cdot\bar{u}_1A)_x=0,$$

which is (2.1).

Next consider $i=1$ in the momentum equation, $a=x$, $b=x+\delta x$. We have similarly with (2.6),

$$\frac{d}{dt}\int_{\Omega(t)}\rho u_1\,dV=\int_{\Omega(t)}(\rho u_1)_t\,dV+\int_{\Omega(t_0)}\rho u_1 J_t\,dV$$

$$=-\int_{\partial\Omega(t)}\rho u_1\vec{u}\cdot\vec{n}\,dS+\int_{\partial\Omega(t)}\sigma_{1,j}\cdot\vec{n}_j\,dS$$

$$+\overline{\rho u_1}A_t\delta x+O(\delta x^2).\qquad(A10)$$

We calculate the integrals of (A10) as

$$\frac{d}{dt}\int_{\Omega}\rho u_1\,dV=(\overline{\rho u_1}A)_t\delta x+O((\delta x)^2)$$

$$\approx(\bar{\rho}\cdot\bar{u}A)_t\cdot\delta x+O((\delta x)^2).\qquad(A11)$$

Using $u_1=0$ on the upper and lower boundaries, a similar calculation as (A8) gives

$$\int_{\partial\Omega}\rho u_1\vec{u}\cdot\vec{n}\,dS=(\bar{\rho}\cdot\bar{u}_1^2 A)|_x^{x+\delta x}+O(\delta x\mu^{1/2}),\qquad(A12)$$

where the smallness of $u_{1,y}$ in the interior and small width of boundary layer $O(\mu^{1/2})$ gives the $O(\mu^{1/2})$ for approximating $\overline{u_1^2}$ by $\overline{u}_1\cdot\overline{u}_1$.

Remark 6.1: Notice that for inviscid flows, we would have an additional term $\bar{\rho}\bar{u}_1A_t\delta x$, which would cancel the third term on the right-hand side of (A10). As a result, the $A_t u/A$ term would be absent from the momentum equation (2.2).

Let us continue to calculate

$$\int_{\partial\Omega}-p\,\delta_{1,j}n_j\,dS\approx-\bar{p}A|_x^{x+\delta x}+\int_x^{x+\delta x}pA_x\,dx$$

$$=-\bar{p}A|_x^{x+\delta x}+\bar{p}A_x\delta x+O((\delta x)^2).$$

Noticing that

$$d_{11}=2\mu(u_{1,x}-(u_{1,x}+u_{2,y})/3),\quad d_{12}=2\mu(u_{1,y}+u_{2,x}).$$

It follows that

$$\overline{d_{11}}=\frac{4}{3}\mu\bar{u}_{1,x}-\frac{2\mu A_t}{3A}.$$

Thus the contribution from the left and right boundaries located at x and $x+\delta x$ is

$$\sum_{l,r}\int_{l,r}d_{11}n_1=A\overline{d_{11}}|_x^{x+\delta x}=\frac{4}{3}A\mu\bar{u}_{1,x}|_x^{x+\delta x}-\frac{2\mu A_t}{3}\Big|_x^{x+\delta x}.\qquad(A13)$$

The contribution from the upper and lower boundaries is

$$\sum_{\pm}\int_{y=\pm A/2}d_{11}n_1\,dS=-d_{11}A_x\delta x/2|_{y=A/2}$$

$$-d_{11}A_x\delta x/2|_{y=-A/2}$$

$$=\mu\delta x\sum_{\pm}O(\partial_y\vec{u})|_{y=\pm A/2}.\qquad(A14)$$

Similarly,

$$\sum_{\pm}\int_{y=\pm A/2}d_{12}n_2\,dS=\mu\delta x\sum_{\pm}O(\partial_y\vec{u})|_{y=\pm A/2}.\qquad(A15)$$

Since $\partial_y \vec{u}|_{y=\pm A/2} = O(\mu^{-1/2})$, the viscous flux from the boundary layers are $O(\delta x \mu^{1/2})$, much larger than the averaged viscous term $\delta x (4\mu/3)(A\overline{u_{1x}})_x = O(\delta x \mu)$. We notice that the vertically averaged quantities have little dependence on the viscous boundary layers unless A is on the order $O(\mu^{1/2})$. Hence the quantities from upper and lower edges in (A14) and (A15), and that in (A12), should balance themselves. Omitting them altogether, and combining remaining terms that involve only $\overline{u}_1$, $\overline{\rho}$ in the bulk, we end up with (after dividing by δx and sending it to zero)

$$(\overline{\rho \cdot u_1}A)_t + (\overline{\rho \cdot u_1^2}A)_x = -(\overline{p}A)_x + A_x \overline{p} + \overline{\rho u_1}A_t$$

$$+ \frac{4\mu}{3}(A\overline{u_{1x}})_x - 2\mu A_{tx}/3, \quad \text{(A16)}$$

which gives the modified Euler (2.2) in the inviscid limit $\mu \to 0$.

APPENDIX B: OSCILLATION MODES NEAR FLAT FOLD

We present a linear analysis of oscillation modes when flow system (2.1)–(2.3) is coupled with a continuous wave model of VF instead of two-mass model. Our objective is to simplify the calculation and understand the VF velocity coupling term $\rho u A_t$. The wave equation is

$$m y_{tt} = \sigma y_{xx} - \alpha y_t - \beta y + p + f_m, \quad \text{(B1)}$$

where σ represents the longitudinal tension, m mass density, α the damping, and β the stiffness. The pressure p acts pointwise on the fold $y = y(t,x) = A(t,x)/2$. The forcing f_m maintains an equilibrium position.

Let us consider the constant (equilibrium) state $(\rho,u,p,y) = (\rho_0,u_0,p_0,y_0)$, $u_0 > 0$, such that

$$-\beta y_0 + p_0 = f_m, \quad p_0 = a^2 \rho_0, \quad \text{(B2)}$$

and a nearby state $u = u_0 + \hat{u}$, $p = p_0 + \hat{p}$, $\rho = \rho_0 + \hat{\rho}$, $y = y_0 + \hat{y}$, where the hat variables are small perturbations. The linearized system is

$$(y_0 \hat{\rho} + \hat{y}\rho_0)_t + (\rho_0 y_0 \hat{u} + \rho_0 u_0 \hat{y} + u_0 y_0 \hat{\rho})_x = 0, \quad \text{(B3)}$$

$$\hat{u}_t + u_0 \hat{u}_x + \frac{1}{\rho_0}\hat{p}_x = \frac{u_0}{y_0}\hat{y}_t, \quad \text{(B4)}$$

$$m\hat{y}_{tt} = \sigma \hat{y}_{xx} - \alpha \hat{y}_t - \beta \hat{y} + \hat{p}. \quad \text{(B5)}$$

Eliminating the $(\hat{\rho},\hat{u},\hat{p})$ variables using (B3) and (B4) and the equation of state $p = a^2 \rho$, we obtain (denoting $\Gamma \equiv a^{-2}$):

$$y_0[\Gamma \partial_{tt} + 2\Gamma u_0 \partial_{xt} + (\Gamma u_0^2 - 1)\partial_{xx}] \cdot (\hat{y}_{tt} - \sigma \hat{y}_{xx} + \alpha \hat{y}_t + \beta \hat{y})$$

$$= -\rho_0[(\partial_t + u_0 \partial_x)^2 \hat{y} + u_0 \hat{y}_t]. \quad \text{(B6)}$$

Seek a mode solution of the form $\hat{y} = e^{imx + \lambda t}$, m real, we end up with the following algebraic equation of degree four for λ:

$$[\Gamma \lambda^2 + 2\Gamma u_0 m \lambda i + (1 - \Gamma u_0^2)m^2] \cdot [\lambda^2 + \sigma m^2 + \alpha \lambda + \beta]$$

$$= -\rho_0 y_0^{-1}[\lambda^2 + 2u_0 im\lambda - u_0^2 m^2] - \frac{u_0 \rho_0 \lambda}{y_0}, \quad \text{(B7)}$$

or

$$\Gamma \lambda^4 + (\alpha \Gamma + 2\Gamma u_0 mi)\lambda^3 + (\Gamma(\beta + \sigma m^2) + 2\alpha \Gamma u_0 mi$$

$$+ \rho_0 y_0^{-1} + (1 - \Gamma u_0^2)m^2)\lambda^2 + \left(2\Gamma u_0 mi(\beta + \sigma m^2)\right.$$

$$\left. - \alpha m^2(\Gamma u_0^2 - 1) + \rho_0 y_0^{-1}(2u_0 im) + \frac{u_0 \rho_0}{y_0}\right)\lambda$$

$$+ [(\beta + \sigma m^2)(1 - \Gamma u_0^2)m^2 + \rho_0 y_0^{-1}(-u_0^2 m^2)] = 0. \quad \text{(B8)}$$

We show the following proposition.

Proposition 7.1: If

$$\rho_0 u_0^2 > \alpha(\rho_0 u_0 + \Gamma \beta u_0 y_0), \quad \text{(B9)}$$

(B8) has a pair of pure imaginary solution $\lambda = \pm i\eta$, $\eta \neq 0$ real, implying the existence of a pair of oscillatory modes to the linearized system (B4) and (B5) of the form $e^{\pm i(mx + \eta t)}$, for real and nonzero numbers m and η.

Proof: Let $\lambda = i\eta$ in (B8), where η is real. The real and imaginary parts give, respectively,

$$\Gamma \eta^4 + 2\Gamma u_0 m \eta^3 - \left[\Gamma(\sigma m^2 + \beta) + m^2(1 - \Gamma u_0^2) + \frac{\rho_0}{y_0}\right]\eta^2$$

$$+ \left[-2\Gamma u_0 m(\beta + \sigma m^2) - \frac{2\rho_0 u_0 m}{y_0}\right]\eta$$

$$+ \left[m^2(1 - \Gamma u_0^2)(\sigma m^2 + \beta) - \frac{2u_0^2 m^2 \rho_0}{y_0}\right] = 0 \quad \text{(B10)}$$

and

$$-\alpha \Gamma \eta^3 - 2\alpha \Gamma u_0 m \eta^2 + m^2 \alpha(1 - \Gamma u_0^2)\eta + \frac{u_0 \rho_0 \eta}{y_0} = 0. \quad \text{(B11)}$$

For $\eta \neq 0$, $\alpha \neq 0$, we have from (B11),

$$\Gamma \eta^2 + 2\Gamma u_0 m \eta - m^2(1 - \Gamma u_0^2) - \frac{u_0 \rho_0}{y_0 \alpha} = 0,$$

so

$$\eta = -u_0 m \pm a\sqrt{m^2 + u_0 \rho_0/(y_0 \alpha)}, \quad \text{(B12)}$$

which is not equal to zero in case of minus sign ($u_0 > 0$). Now we regard the left-hand side of (B11) as a continuous function of m, call it $F(m)$. For $|m| \gg 1$, $\eta \sim (-u_0 - a)m$, direct calculation shows

$$F(m) \sim -\frac{\rho_0}{\Gamma y_0}m^2 < 0.$$

While for $|m| \ll 1$,

$$\eta \sim -\sqrt{\frac{u_0 \rho_0}{\Gamma y_0 \alpha}} + O(m),$$

$$F(m) \sim \frac{u_0 \rho_0}{\Gamma y_0 \alpha}\left(\frac{u_0 \rho_0}{y_0 \alpha} - \Gamma \beta - \frac{\rho_0}{y_0}\right) > 0,$$

provided

$$\frac{u_0 \rho_0}{y_0} > \alpha\left(\frac{\rho_0}{y_0} + \Gamma \beta\right), \quad \text{(B13)}$$

J. Acoust. Soc. Am., Vol. 114, No. 1, July 2003

LaMar *et al.*: Modeling vocal fold motion   463

holds, which is just (B9). Under (B9), $F(m)=0$ has a non-zero real solution, hence an oscillatory mode solution exists to (B10) and (B11). Finally, noticing that equations (B10) and (B11) are invariant under the symmetry transform $(\eta,m) \rightarrow (-\eta,-m)$, we conclude that the oscillatory modes exist as a pair.

Remark 7.1: Condition (B9) *says that the fluid energy must be large enough to overcome the fold damping due to α. Without the term $\rho u A_t$ in (2.2), the same calculation would show that $F(m) = -\rho_0 m^2/(\Gamma y_0) < 0$ for all m, implying non-existence of oscillatory mode. Condition (B9) is similar to the threshold pressure in Titze's wave model[19] in the sense that minimum energy (analogous to minimum lung pressure) is proportional to the fold damping coefficient and the pre-phonatory half-width.*

[1] K. Ishizaka and J. L. Flanagan, "Synthesis of voiced sounds from a two-mass model of the vocal cords," AT&T Tech. J. **51**, 1233–1268 (1972).

[2] I. Bogaert, "Speech production by means of a hydrodynamic model and a discrete-time description," Inst Perception Res, Einhoven, the Netherlands, Report no. 1000, 1994.

[3] B. Story and I. Titze, "Voice simulation with a body-cover model of the vocal folds," J. Acoust. Soc. Am. **97**, 1249–1260 (1995).

[4] I. Titze, "The human vocal cords: A mathematical model, part I," Phonetica **28**, 129–170 (1973).

[5] I. Titze, "The human vocal cords: A mathematical model, part II," Phonetica **29**, 1–21 (1974).

[6] F. Alipour and R. Scherer, "Vocal fold bulging effects on phonation using a biophysical computer model," J. Voice **14**, 470–483 (2000).

[7] F. Alipour, D. Berry, and I. Titze, "A finite-element model of vocal fold vibration," J. Acoust. Soc. Am. **108**, 3003–3012 (2000).

[8] X. Pelorson, A. Hirschberg, A. Wijnands, and H. Bailliet, "Description of the flow through *in-vitro* models of the glottis during phonation," Acta Acust. (Beijing) **3**, 191–202 (1995).

[9] J. Flanagan, *Speech Analysis, Synthesis and Perception*, 2nd ed. (Springer-Verlag, New York, Berlin, 1972).

[10] L. Mongeau, N. Franchek, C. Coker, and R. Kubil, "Characteristics of a pulsating jet through a small modulated orifice, with applications to voice production," J. Acoust. Soc. Am. **102**, 1121–1132 (1997).

[11] G. B. Whitham, *Linear and Nonlinear Waves* (Wiley, New York, 1974).

[12] T.-P. Liu, "Transonic gas flow in a duct of varying area," Arch. Ration. Mech. Anal. **80**, 1–18 (1982).

[13] T.-P. Liu, "Nonlinear stability and instability of transonic flows through a nozzle," Commun. Math. Phys. **83**, 243–260 (1982).

[14] R. Menikoff, K. Lackner, N. Johnson, S. Colgatem, J. Hyman, and G. Miranda, "Shock wave driven by a phased implosion," Phys. Fluids A **3**, 201–218 (1991).

[15] I. Titze, "Current topics in voice production mechanisms," Acta Oto-Laryngol. **113**, 421–427 (1993).

[16] J. Jiang and I. Titze, "Measurement of vocal fold intraglottal pressure and impact stress," J. Voice **8**, 132–144 (1994).

[17] K. Stevens, *Acoustic Phonetics* (MIT, Cambridge, MA, 2000).

[18] R. Leveque, *Numerical Methods for Conservation Laws* (Birkhauser-Verlag, Basel, 1990).

[19] I. Titze, "The physics of small-amplitude oscillation of the vocal folds," J. Acoust. Soc. Am. **83**, 1536–1552 (1988).

[20] J. Golub and J. Ortega, *Scientific Computing and Differential Equations* (Academic, New York, 1992).

[21] R. Sataloff, "The human voice," Sci. Am. **1992**, 108–115 (1992).

[22] S. Austin and I. Titze, "The effect of subglottal resonance upon vocal fold vibration," J. Voice **11**, 391–402 (1997).

[23] G. Batchelor, *Introduction to Fluid Mechanics* (Cambridge U.P., Cambridge, MA, 1980).